COMPARATIVE STUDY OF METHODS FOR CALCULATING THE AERODYNAMIC LIFTING SURFACES IN SUBSONIC REGIME UNDER CHORD AND INCIDENCE CHANGES

Corneliu BERBENTE[1], Marwan ISBER[2], Daniel CRUNTEANU[3]

Articolul prezintă trei metode pentru calculul aerodinamic asupra unui aripi cu anvergura finită în regim incompresibil şi nevascos insistand asupra unui metode orginale dezvoltate în anii 70 care este utilizată si acum. Metodele clasice cu panouri, (lattice vortex method) cu inele de vârtej si cu potcoave de vârtej sunt prezentate şi folosite pentru calculul a patru configuraţii de aripă. Rrezultatele obtinute cu aceste două metode sunt comparate cu rezultatele metodei semi-analitice şi interpretarea rezultatelor este prezentată în capitolul de concluzii.

The paper presents three methods to compute the incompressible non-viscous flow for wings with arbitrary plan-form, insisting on an original method, developed in the 70's, currently under usage. The classical methods of vortex lattice methods (panels) in two variants, namely ring and horseshoe, are presented and used to compute four wing configurations. Further, results obtained with these two methods are compared with the semi-analytical method. The findings are presented in the conclusion.

Incidence = angle of atack

Keywords: VLM, vortex lattice method, semi-analytical method, panel method

1. Introduction

The paper presents classical VLM methods developed and employed in [6], [9], [12] and [13], as well as an original method presented in [1]. Results obtained with these ring-vortex and horseshoe VLM methods are compared with results from the original semi-analytical method in [1].

The purpose of this work is to compare these methods for two classes of wings: low aspect ratio ($\lambda = 2$) and moderate aspect ratio ($\lambda = 6$) and identify the trust areas for each method.

[1] Prof., Aerospace Engineering Faculty, University POLITEHNICA of Bucharest, Romania
[2] PhD. Stud. Aerospace Engineering Faculty, University POLITEHNICA of Bucharest, Romania, email: marwan_jb@yahoo.com
[3] PhD. Stud. ,Teaching Assistant ,Aerospace Engineering Faculty, University POLITEHNICA of Bucharest, Romania

Chapter 2 presents the ring VLM method (MIV), Chapter 3 the horseshoe VLM (MPV), Chapter 4 the semi-analytical method (MSA). Results are presented in Chapter 5 and conclusions in Chapter 6.

2. Lifting surface method which using rings vortices

The flow is considered potential, incompressible. The potential can be deduced, using the Green function as:

$$\Phi\left(\bar{x}_P\right)=\frac{1}{4\pi}\int_{S_C}\left[\sigma\frac{1}{r}-\mu\frac{\partial}{\partial n}\left(\frac{1}{r}\right)\right]ds+\frac{1}{4\pi}\int_{S_R}\left[-\mu\frac{\partial}{\partial n}\left(\frac{1}{r}\right)\right]ds+\Phi_\infty\left(\bar{x}_P\right) \qquad (1)$$

Where :

$\sigma=\dfrac{\partial\Phi}{\partial n}-\dfrac{\partial\Phi_{\text{int}}}{\partial n}$ intensity of distributed sources

$\mu=\Phi-\Phi_{\text{int}}$ intensity distribution

Φ velocity potential near the surface

Φ_{int} velocity potential inside the body

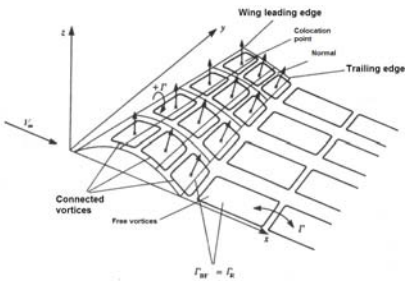

Fig. 1 Global wing paneling [7]

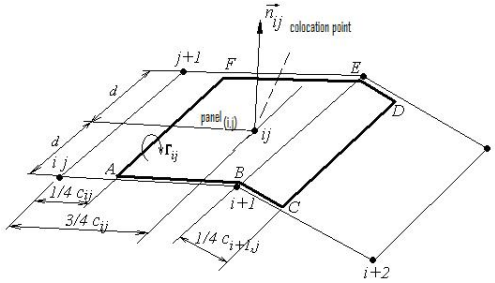

Fig. 2 Modeling the wing with ring vortices [7]

The ring vortex (Fig. 2) induces a velocity :

$$\vec{V}_P=\frac{\Gamma}{4\pi}\oint_{C_i}\frac{\vec{r}\times d\vec{r}}{r^3} \qquad \vec{V}_p=\frac{\Gamma}{4\beta\pi d}\left(\cos\alpha+\cos\beta\right)\cdot\vec{d}_V \quad (2)$$

[7]

where:

$$\cos\alpha=\frac{\overrightarrow{AP}\cdot\overrightarrow{AB}}{AP\cdot AB}\ ,\ \cos\beta=\frac{\overrightarrow{BA}\cdot\overrightarrow{BP}}{AB\cdot BP}\ ,\ \vec{d}_V=\frac{\overrightarrow{AB}\times\overrightarrow{AP}}{\left|\overrightarrow{AB}\times\overrightarrow{AP}\right|} \quad (3)$$

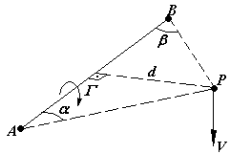

Fig. 3 Induced velocity of a vortex line [7]

In order to obtain the intensities of the ring vortices $\Gamma_{i,j}$ one takes into account that the total velocity of point P is tangent to the lifting surface:

$$\left(\sum_{i=1}^{M} \sum_{j=1}^{N} \left(\vec{V}_{ind,P} \left(\Gamma_{i,j} \right) \right)_{i,j} + \sum_{i=1}^{M_w} \sum_{j=1}^{N} \left(\vec{V}_{w,P} \left(\Gamma_{i,j} \right) \right)_{i,j} \right) \cdot \vec{n}_P = -\vec{V}_\infty \cdot \vec{n}_P \text{ [7],} \quad (4)$$

where: M is the number of panels in the chord-wise , N is the number of panels in span-wise and M_w is the number of rings in each subdivision of the wake. The wake surface length is equal to three wing spans.

The Biot-Savart formula for calculation of the induced velocity leads to singularity when the distance between collocation and vortex line tends to zero. This leads to unrealistic big induced velocity, having some consequences: disturbed local angle of attack, overestimated induced velocities near wingtips. Therefore we obtain a numerically unrealistic solution. In order to avoid these numerical disturbances, a finite radius vortex core has been used. The flow field generated by this vortex corresponds to a solid body rotation, referring to the tangential velocity. Fig. 4 contains the formulation and representation of the tangential velocity.

$$v_\theta \left(r \right) = \frac{\Gamma \cdot r}{2\pi \left(r_c^{2n} + r^{2n} \right)^{1/n}} \quad (5)$$

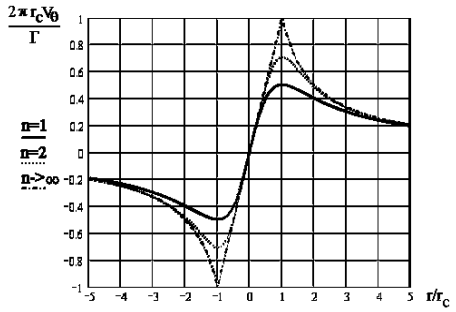

Fig. 4 Dimensionless tangential velocity profile[7]

Setting $n \to \infty$, the Rankine velocity profile is obtained and this model is used in our approach.

The core radius is proportional to $10^{-4} \cdot \sqrt{A}$, where A is panel area.

By using the Kutta-Jukovski theorem, we obtain the lifting force acting on the current panel: $\Delta P_{i,j} = \rho V_\infty \left(\Gamma_{i,j} - \Gamma_{i-1,j} \right) \Delta y_{i,j}, i > 1$ (6), while for the leading edge panel we obtain $\Delta P_{1,j} = \rho V_\infty \Gamma_{1,j} \Delta y_{1,j}$ (7).

The pressure difference between the panel surfaces will be given by $\Delta p_{i,j} = \frac{\Delta P_{i,j}}{S_{i,j}}$ (8), where S is the panel area.

To compute the induced drag, we use:

$$\begin{aligned} \Delta R_{i,j} &= -\rho w_{ind_{i,j}} \left(\Gamma_{i,j} - \Gamma_{i-1,j}\right)\Delta y_{i,j} \text{ , } i > 1 \\ \Delta R_{1,j} &= -\rho w_{ind_{1,j}} \Gamma_{1,j} \Delta y_{1,j} \end{aligned} \tag{9}$$

where the velocity component $w_{ind_{i,j}}$ must be locally calculated.

The unitary coefficients of lift and drag are:

$$C_z = \frac{\sum_{i=1}^{M}\sum_{j=1}^{N} \Delta P_{i,j}}{\rho V_\infty^2 S/2} \text{ , } C_{xi} = \frac{\sum_{i=1}^{M}\sum_{j=1}^{N} \Delta R_{i,j}}{\rho V_\infty^2 S/2} \tag{10}$$

3. Lifting surface method using horseshoe vortex

This simplified model is used in order to have an additional model to compare with lifting surface method using ring vortices and with semi-analytical method.

The model is described by the fact that each panel has a horseshoe assigned, as in Fig. 5. The finite segment of the horseshoe is placed at ¼ of the panel's chord and the collocation point at ¾. The infinite segments of the horseshoe are parallel to the free-stream velocity.

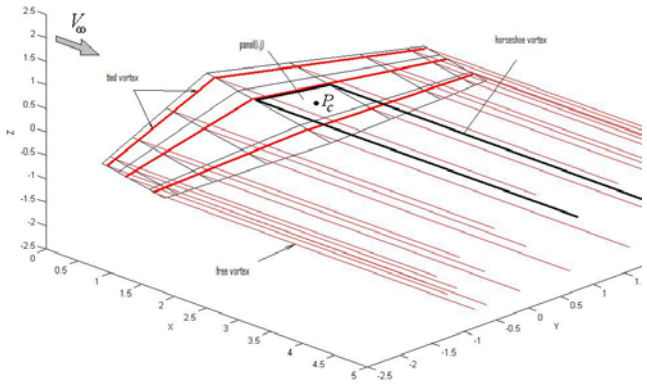

Fig. 5 Lifting surface method which using horseshoe vortex model

As presented before, in the case of ring vortices method, the lifting force acting on the current panel is $\Delta P_{i,j} = \rho V_\infty \Gamma_{i,j} \Delta y_{i,j}$.

The pressure difference for the panel is: $\Delta p_{i,j} = \frac{\Delta P_{i,j}}{S_{i,j}}$ where S is the panel area.

The induced drag of the panel is $\Delta R_{i,j} = -\rho w_{ind_{i,j}} \Gamma_{i,j} \Delta y_{i,j}$ and the unitary coefficients are the same as in the case of ring vortices method.

All the above are used to perform the calculations in the tests chosen for methods comparisons.

4. The semi-analytical method

The Prandtl's integral-differential equation

$$\Gamma = kcV_\infty \left(\alpha - \frac{1}{4\pi V_\infty} \int_{-\frac{b}{2}}^{\frac{b}{2}} \frac{d\Gamma}{dy'} \cdot \frac{dy'}{y - y'} \right) \tag{11},$$

where c is the local chord, is solved starting with a Fourier development of the circulation

$$\Gamma = 2bV_\infty \sum_{n=1}^{\infty} A_n \sin n\theta \ , \quad y = -\frac{b}{2}\cos\theta \ , \tag{12}$$

$\theta \in [0, \pi]$, where b is the wing span, having as result an infinite system of linear equations.

Our method has some advantages like: a) the integrals can be calculeted exactly for current cases, b) the process of calculating the coeffiecients is based on successive iteration and c) the first approximation is obtained with an explicit formulation;

One obtains the circulation coefficients from:

$$\sum_{n=1}^{\infty} A_n \sin n\theta = \mu \left(\alpha - \sum_{n=1}^{\infty} \frac{nA_n \sin n\theta}{\sin\theta} \right) \tag{13}$$

equation that comes from introducing the Fourier development of circulation in the Prandtl equation, where,

$$\mu = kc/(2b) \quad k = (0{,}85...0{,}9)\pi \ .$$

Multiplying Eq. 13 with $\sin(n\theta)$ and integrating from 0 to π, we get

$$\frac{\pi}{2} A_n = I_n - \sum_{p=1}^{\infty} pH_{np} A_p, \quad n = 1,2,3,... \tag{14}$$

After solving for A_n

$$\left(\frac{\pi}{2}+nH_{nn}\right)A_n = I_n - \sum_{p=1}^{\infty} p\left(1-\delta_{np}\right)H_{np}A_p, \quad n=1,2,3,... \tag{15}$$

$$I_n = \int_0^{\pi} \mu\alpha \sin n\theta \; d\theta, \quad H_{np} = H_{pn} = \int_0^{\pi} \frac{\mu \sin n\theta \; \sin p\theta}{\sin\theta} \; d\theta \tag{16}$$

where δ_{np} is the Kronecker symbol $\delta_{np} = \begin{cases} 1, & n = p \\ 0, & n \neq p \end{cases}$.

The integrals I_n and H_n can be calculated directly, whatever complicated distribution would be in chord or incidence, without the necessity of developing them in Fourier series.

The wing is symmetrical and therefore

$$\mu(\theta) = \mu(\pi - \theta); \quad H_{np} = 0 \tag{17}$$

"$n+p$" being an odd number.

This allows a separation in the A_n coefficients calculation ,after the parity of the index. We note with:

$$L_n = \frac{\pi}{2} + nH_{nn} \tag{18}$$

The system is decomposed into two systems:

$$L_{2m-1}A_{2m-1} = I_{2m-1} - \sum_{p=1}^{\infty}(2p-1)\left(1-\delta_{mp}\right)H_{2m-1,2p-1}A_{2p-1}$$

$$L_{2m}A_{2m} = I_{2m} - \sum_{p=1}^{\infty} 2p\left(1-\delta_{mp}\right)H_{2m,2p}A_{2p}, \quad m=1,2,3,... \tag{19}$$

To find the coefficients A_{2m-1} or A_{2m}, the following series of successive approximations are used:

a) in the first approximation we neglect the term A_{2m+3} and the next terms, when computing A_{2m-1}

b) in the approximation with the order $s \geq 2$ we calculate the terminal A_{2m-1} taking in the consideration all the calculated terms in the previous approximations, including $A_{2m+4s-3}$.

The first approximation is:

$$L_{2m-1}A_{2m-1} + (2m+1)H_{2m+1,2m-1}A_{2m+1} = I_{2m+1} - \sum_{p=1}^{m-1}(2p-1)H_{2m-1,2p-1}A_{2p-1}$$

$$(2m-1)H_{2m+1,2m-1}A_{2m-1} + L_{2m+1}A_{2m+1} = I_{2m+1} - \sum_{p=1}^{m-1}(2p-1)H_{2m+1,2p-1}A_{2p-1} \tag{20}$$

where we have:

$$A_{2m-1}^{(1)} = \frac{M_{2m-1} - \sum_{p=1}^{m-1} N_{2m-1,2p-1} A_{2p-1}^{(1)}}{P_{2m-1}}$$

$$P_{2m-1} = L_{2m-1}L_{2m+1} - \left(4m^2 - 1\right) H_{2m+1,2m-1}^2 \tag{21}$$

$$N_{2m-1,2p-1} = (2p-1)\left[L_{2m+1}H_{2m-1,2p-1} - (2m+1) H_{2m+1,2m-1}H_{2m+1,2p-1} \right]$$

$$M_{2m-1} = I_{2m-1}L_{2m+1} - (2m+1) H_{2m+1,2p-1}I_{2m+1} \tag{22}$$

Approximations with rank $s \geq 2$ will use:

$$A_{2m-1}^{(s)} = \frac{I_{2m-1} - \sum_{p=1}^{m+2s-1} (2p-1)\left(1-\delta_{mp}\right) H_{2m-1,2p-1} A_{2p-1}^{(s-1)}}{L_{2m-1}} \tag{23}$$

For the even index coefficients A_{2m}, we apply a similar procedure.

Since coefficients A_n decrease rapidly, the process is rapidly convergent; even the first approximation gives a good accuracy.

Assuming a picewise linear chord and angle of attack distribution between sections y_i and y_{i+1},

$$c(\theta) = c_i + \frac{c_{i+1} - c_i}{\cos\theta_{i+1} - \cos\theta_i}\left(\cos\theta - \cos\theta_i\right) = C_i + D_i \cos\theta \tag{24}$$

$$\alpha(\theta) = \alpha_i + \frac{\alpha_{i+1} - \alpha_i}{\cos\theta_{i+1} - \cos\theta_i}\left(\cos\theta - \cos\theta_i\right) = E_i + F_i \cos\theta \tag{25}$$

then the integrals I and H will have the form

$$I_{2m-1} = \frac{k}{b}\sum_{i=1}^{n_s-1}\left(\begin{array}{l} C_iE_i\int_{\theta_i}^{\theta_{i+1}} \sin(2m-1)\theta\, d\theta + (C_iF_i + D_iE_i)\int_{\theta_i}^{\theta_{i+1}} \sin(2m-1)\theta\cos\theta\, d\theta + \\ + D_iF_i\int_{\theta_i}^{\theta_{i+1}} \sin(2m-1)\theta\cos^2\theta\, d\theta \end{array} \right) \tag{26}$$

$$H_{2m-1,p} = \frac{k}{b}\sum_{i=1}^{n_s-1}\left(C_i\int_{\theta_i}^{\theta_{i+1}} \frac{\sin(2m-1)\theta\,\sin p\theta}{\sin\theta}\, d\theta + D_i\int_{\theta_i}^{\theta_{i+1}} \frac{\sin(2m-1)\theta\,\sin p\theta}{\sin\theta}\cos\theta\, d\theta \right) \tag{27}$$

where $\theta_1 = 0$, $\theta_{ns} = \pi/2$ and n_s – number of computing sections.

5. Numerical results

In order to test the methods, some calculations have been performed on two types of trapezoidal wings (zero degrees for the ¼ chord line), considering

aspect ratios $\lambda = 2$ and $\lambda = 6$. Free-stream velocity is 100m/s and density 1.225Kg/m^3. The trapezoidal shape coefficient is $q = 1 - c_e / c_0$.

Small aspect ratio wing $\lambda = 2,\ b = 2\ m,\ S = 2\ m^2$

Case 1. $q = 0,\ c_0 = c_e = 1\ m,\ \alpha = 4^0$

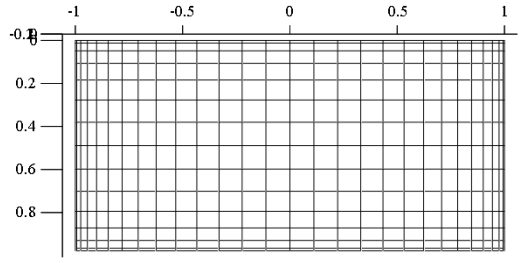

Fig.6 Discretized wing with 15 x 29 panels for (MPV and MIV)

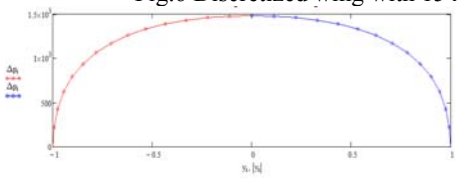

Fig.7 Lift distribution MSA (semi-analytical method)

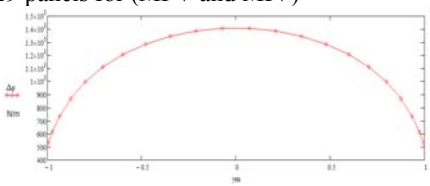

Fig.8 Lift distribution MIV (vortex rings)

	Cz			Cxi		
a	MSA	MPV	MIV	MSA	MPV	MIV
0	0,00000	0,00000	0,00000	0,00000	0,00000	0,00000
2	0,10060	0,10183	0,10082	0,00163	0,00323	0,00320
4	0,20110	0,21300	0,20480	0,00652	0,01351	0,01280
6	0,30170	0,31140	0,30279	0,01470	0,03163	0,02874
8	0,40220	0,41430	0,41120	0,02606	0,05824	0,05103
10	0,50280	0,52460	0,51542	0,04072	0,09385	0,07960
12	0,60340	0,64895	0,64100	0,05864	0,13903	0,11425

MSA semi-analytical method
MPV horseshoe vortex method
MIV ring vortex method

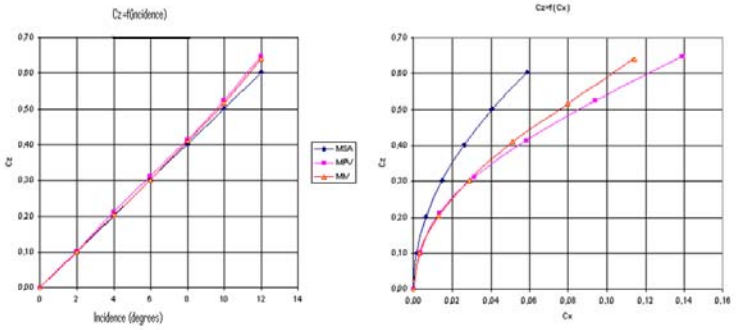

Fig. 9 Lift curves, lift and drag curves for rectangular wing, $\lambda = 2$

Case 2. $q = 0.5,\ c_0 = 1.333\,m,\ c_e = 0.667\ m,\ \alpha = 4^0$

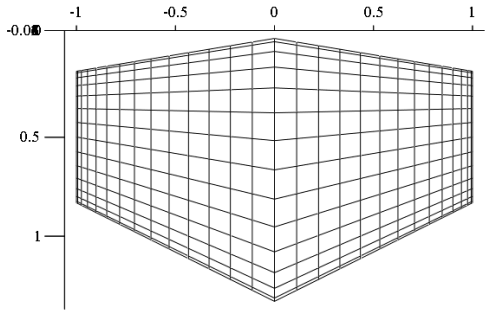

Fig.10 Discretized wing with 15 x 29 panels for(MPV and MIV)

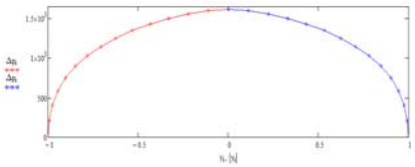

Fig.11 Lift distribution MSA

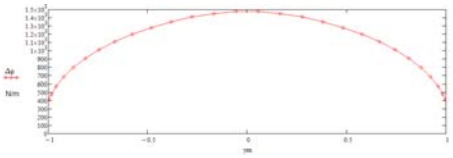

Fig.12 Lift distribution MIV

	Cz			Cxi		
a	MSA-trap.	MPV-trap.	MIV-trap.	MSA-trap.	MPV-trap.	MIV-trap.
0	0,00000	0,00000	0,00000	0,00000	0,00000	0,00000
2	0,10340	0,11283	0,10582	0,00170	0,00324	0,00324
4	0,20690	0,22300	0,21580	0,00682	0,01346	0,01300
6	0,31030	0,32140	0,31279	0,01533	0,03140	0,02932
8	0,41370	0,42430	0,41920	0,02725	0,05758	0,05230
10	0,51710	0,53460	0,52742	0,04258	0,09265	0,08190
12	0,61060	0,66095	0,65500	0,05937	0,13700	0,11800

MSA- semi analytical method
MPV- horseshoe vortex method
MIV- ring vortex method

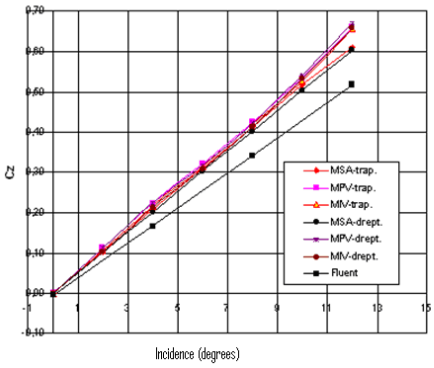

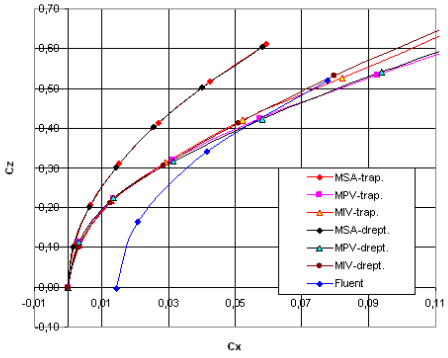

Fig. 13 Lift curves, lift and drag curves for trapezoidal wing, $\lambda = 2$

Moderate aspect ratio wing $\lambda = 6,\ b = 6\ m,\ S = 6\ m^2$

Case 1. $q = 0,\ c_0 = c_e = 1\ m,\ \alpha = 4^0$

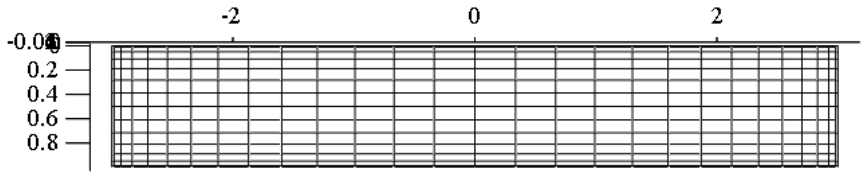

Fig.14 Discretized wing with 15 x 29 panels for (MPV and MIV)

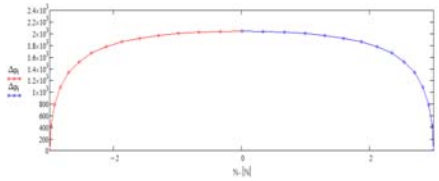

Fig.15 Lift distribution MSA

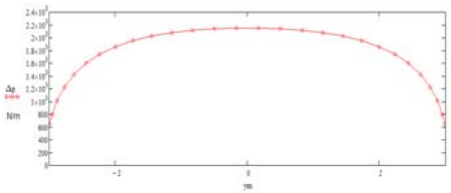

Fig.16 Lift distribution MIV

	Cz			Cxi		
a	MSA-drept	MPV-drept	MIV-drept	MSA-drept	MPV-drept	MIV-drept
0	0	0	0	0	0	0
2	0.1468	0.1509	0.15381	0.001143856	0.001265	0.001408
4	0.294	0.3051	0.307	0.004587898	0.005171	0.00561
6	0.44	0.4623	0.4589	0.010276008	0.011873	0.012535
8	0.5872	0.6225	0.6088	0.01830169	0.021528	0.022062
10	0.734	0.7856	0.756	0.028596391	0.034287	0.03402
12	0.881	0.95112	0.8997	0.041197505	0.050257	0.048182

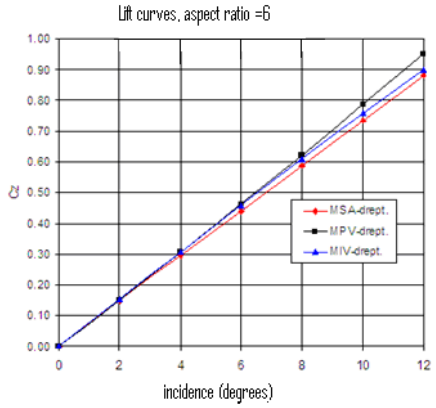

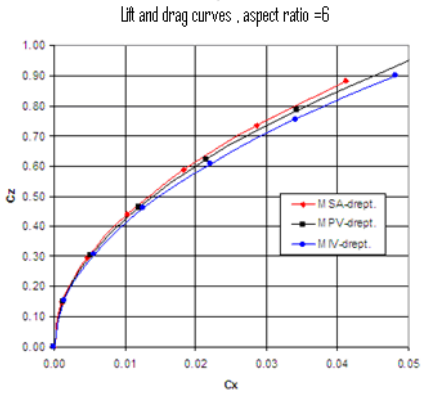

Fig. 17 Lift curves, lift and drag curves for rectangular wing, $\lambda = 6$

Case 2. $q = 0.5,\ c_0 = 1.333\,m,\ c_e = 0.667\ m,\ \alpha = 4^0$

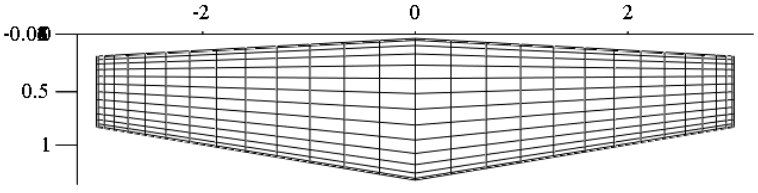

Fig.18 Discretized wing with 15 x 29 panels for (MPV and MIV)

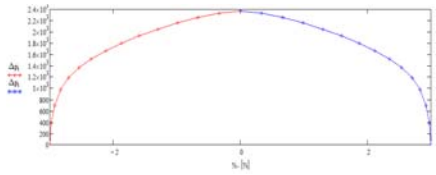

Fig.19 Lift distribution MSA

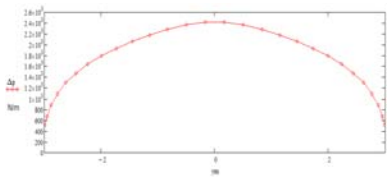

Fig.20 Lift distribution MIV

	Cz			Cxi		
a	MSA-trap.	MPV-trap.	MIV-trap.	MSA-trap.	MPV-trap.	MIV-trap.
0	0	0	0	0	0	0
2	0.1511	0.155	0.1582	0.001039	0.001144	0.001233
4	0.3023	0.312	0.3159	0.004158	0.004635	0.004916
6	0.4534	0.471	0.4722	0.009353	0.010564	0.010984
8	0.6046	0.63262	0.6267	0.016631	0.019058	0.019347
10	0.756	0.7965	0.7786	0.026003	0.03021	0.029863
12	0.907	0.9624	0.927	0.037427	0.044105	0.042331

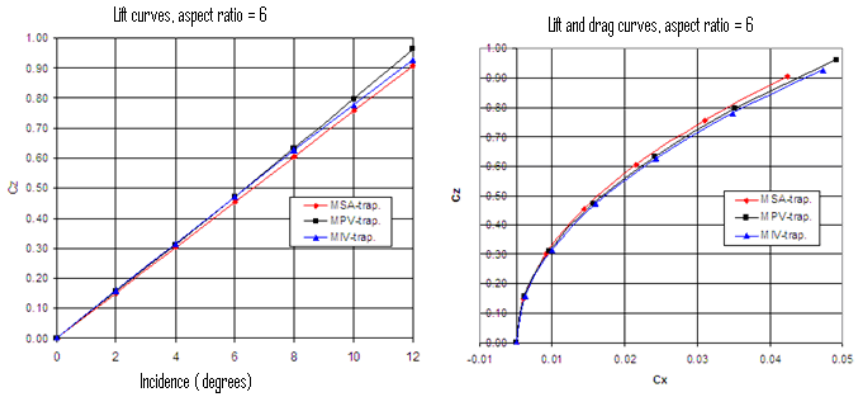

Fig. 21 Lift curves, lift and drag curves for trapezoidal wing, $\lambda = 6$

Table 1

Small aspect ratio wing results

λ=2, α=4^0	C_z			$C_{x,i}$		
q	MSA	MPV	MIV	MSA	MPV	MIV
0	0.2011	0.1938	0.1828	0.006516	0.01351	0.01280
0.5	0.2069	0.1930	0.1858	0.006828	0.01346	0.01299

Table 2

Moderate aspect ratio wing results

λ=6, α=4^0	C_z			$C_{x,i}$		
q	MSA	MPV	MIV	MSA	MPV	MIV
0	0.2942	0.3051	0.3070	0.004833	0.02125	0.02147
0.5	0.3023	0.3121	0.3159	0.004920	0.02172	0.02292

6. Conclusions

For the wings with small aspect ratio $\lambda = 2$, all three methods give good results for lifting coeficients C_z, while there is a difference in the induced drag

prediction. Panel methods (MPV and MIV) oversestimate the value of drag coefficient, the presented semi-analytical method MSA being a good alternative for small aspect ratios. MSA can be further applied for different kind of vehicles: rockets and missile low aspect ratio wings at low velocity, helicopter wings and tail, with better resolution than normal VLM tools.

For the wings with moderate aspect ratio $\lambda = 6$, all three methods give more or less the same coefficients.

The lift and drag coefficients do not change significatly with the trapezoidality coefficient q.

Two problems will be the goals of future work: the implementation of these methods in compressible, viscous flows and their coupling with more advansed methods for the preliminary design phase when aerodynamic configuration is under consistent geometric changes.

R E F E R E N C E S

[1] *Berbente Corneliu*, Asupra unei metode pentru calculul aerodinamic al aripilor de anvergura finita in regim incompresibil (On the method of aerodynamic calculus of the finite wingspan wings in incomressible regime) Buletinul Institutului Politehnic, tomul XXXV-1973, nr. 5.

[2] *C.A. Brebbia, J.C.F.Telles, L.C.Wrobel*, Boundary Element Techniques, Springer-Verlag, New York, 1984

[3] *Caius Iacob,* Introduction mathematique a la mecanique des fluides, 1959

[4] *Carafoli Elie*, Aerodinamica (Aerodynamics), Ed. Tehnică, 1951.

[5] *H. Dumitrescu, V. Cardos, F. Frunzulică, A. Dumitrache*, Aerodinamica nestaționară, aeroelasticitate si aeroacustica pentru turbine de vant (Non steady aerodynamics, aeroelasticity and aeroacoustics of wind turbines) , Ed. Academiei Romne 2007.

[6] *J.L. Hess*, Calculation of potential flow about arbitrary three-dimensional lifting bodies, Tehnical Report, Douglas Aircraft Company, 1969

[7] *J Katz, A. Plotkin*, Low-Speed Aerodynamics, Cambridge University Press 2001

[8] *R. Legendre,* Enroulement de nappes de tourbillons issues de contours de surfaces portantes, La Recherche Aerospatiale, 1981 – 3

[9] *B. Maskew,* Prediction of Subsonic Aerodynamic Characteristics: A Case for Low-Order Panel Methods, AIAA J., 19, 2, 1982

[10] *L. Morino, L.T. Chen, E.O. Suciu*, Steady and Oscillatory Subsonic and Supersonic Aerodynamics Around Complex Configurations, AIAA J., 13, 3, 1975

[11] *L. Morino, Ching-Chiang Kuo,* Subsonic Potential Aerodynamics for Complex configurations: A General Theory, AIAA J., 12, 2, 1974

[12] *C. Rehbach*, Calcul numerique d'ecoulements tridimensionels instationnaires avec nappes tourbillonnaires, La Recherche Aerospatiale, 1977 - 5

[13] *T.D. Rubin– Lopan,* A low-order panel method for subsonic and supersonic flows, The AERONAUTICAL Journal, 93, 925, May 1989

[14] *D. M. Stoia, F. Frunzulica,* About A Low-Order Panel Method for Compressible Flows, Computing, 1, 1996